

# Shape, shear & flexion: An analytic flexion formalism for realistic mass profiles <sup>\*</sup>

P. D. Lasky<sup>1†</sup> and C. J. Fluke<sup>1‡</sup>

<sup>1</sup>Centre for Astrophysics & Supercomputing, Swinburne University of Technology, PO Box 218, Hawthorn, Victoria, 3122, Australia

25 April 2022

## ABSTRACT

Flexion is a non-linear gravitational lensing effect that arises from gradients in the convergence and shear across an image. We derive a formalism that describes non-linear gravitational lensing by a circularly symmetric lens in the thin-lens approximation. This provides us with relatively simple expressions for first- and second-flexion in terms of only the surface density and projected mass distribution of the lens. We give details of exact lens models, in particular providing flexion calculations for a Sérsic-law profile, which has become increasingly popular over recent years. We further provide a single resource for the analytic forms of convergence, shear, first- and second-flexion for the following mass distributions: a point mass, singular isothermal sphere (SIS); Navarro-Frenk-White (NFW) profile; Sérsic-law profile. We quantitatively compare these mass distributions and show that the convergence and first-flexion are better indicators of the Sérsic shape parameter, while for the concentration of NFW profiles the shear and second-flexion terms are preferred.

**Key words:** gravitational lensing – galaxies: halos – dark matter

## 1 INTRODUCTION

Quantifying the exact shape of baryonic and dark matter density profiles that form in expanding  $\Lambda$ CDM cosmologies is an ongoing issue. N-body simulations suggest that CDM halos are well fitted by either Navarro-Frenk-White (NFW) density profiles (Navarro et al. 1997) or de-projected *Sérsic-like* laws in the form of Einasto (1965) or Prugniel & Simien (1997) density profiles (Navarro et al. 2004; Merritt et al. 2005, 2006; Graham et al. 2006a,b). Numerous observations of early-type galaxies suggest their luminosity profiles, and hence stellar mass distributions, follow either Sérsic, core-Sérsic or Nuker-law models (e.g. Lauer et al. 1995, 2005; Graham et al. 2003; Ferrarese et al. 2006; Côté et al. 2006, and references therein), while gravitational lensing observations have suggested the *total* mass distribution (i.e. baryons plus dark matter) is consistently described by isothermal spheres (Treu & Koopmans 2002, 2004; Rusin et al. 2003; Rusin & Kochanek 2005; Koopmans et al. 2006; Gavazzi et al. 2007; Czoske et al. 2008; Dye et al. 2008; Tu et al. 2009). Meanwhile, debate about the mass distributions of galaxy clusters has

been no less intense; only recently is the NFW profile (e.g. Carlberg et al. 1997; van der Marel et al. 2000; Athreya et al. 2002; Katgert et al. 2004; Lin et al. 2004; Hansen et al. 2005; Lokas et al. 2006; Rines & Diaferio 2006; Wojtak et al. 2007; Okabe et al. 2009) being favoured over the isothermal sphere (e.g. Athreya et al. 2002; Etori et al. 2002; Katgert et al. 2004). As gravitational lensing traces total projected mass, it is an extremely powerful tool for determining the mass distributions of these systems without having to make assumptions about the dynamics or constitution of the lensing objects (for recent reviews see Schneider 2005; Hoekstra & Jain 2008).

Traditionally, the study of weak lensing has been limited to linear effects; convergence and shear. These fields have the effect that an elliptically shaped source galaxy gets mapped to an elliptical image. Therefore, to determine information about the lensing object using first-order quantities, assumptions must be made about the intrinsic ellipticity of the source galaxy, or a large number of source galaxies must be utilised to ensure statistically reasonable results can be inferred (see for e.g. Hoekstra et al. 2004; Mandelbaum et al. 2006). Recently however, various authors have begun to consider higher-order lensing effects known as flexion (Goldberg & Natarajan 2002; Goldberg & Bacon 2005; Bacon et al. 2006)<sup>1</sup>. Flexion comes

<sup>\*</sup> Research undertaken as part of the Commonwealth Cosmology Initiative (CCI:www.thecci.org), an international collaboration supported by the Australian Research Council

<sup>†</sup> E-mail: plasky@astro.swin.edu.au

<sup>‡</sup> E-mail: cfluke@astro.swin.edu.au

<sup>1</sup> Irwin & Shmakova (2005, 2006) also consider higher-order lens-

in two flavours that correspond to various spatial derivatives of the shear and convergence, implying they are due to gradients in the first-order fields across the extent of the source/image. Physically, one can think of first-flexion as a shift in the centroid of the image with respect to the source and second-flexion as creating an arc-like structure in the image (Bacon et al. 2006). That is, with the inclusion of flexion, an elliptical source galaxy gets mapped to a “jelly-bean” shaped image for a circularly symmetric lens. In this way, flexion provides a better observable than the first-order fields as only one reasonable assumption about the source galaxy is required – i.e. galaxies are not intrinsically flexed<sup>2</sup>.

The flexion of a lensed image is formally calculated using multipole moments (Goldberg & Natarajan 2002; Goldberg & Leonard 2007; Okura et al. 2007, 2008), however in this work we choose to treat the gravitational lensing variables as field variables. That is, we determine the amount of convergence, shear and flexion one would measure as a function of the distance from the centre of the lensing mass and the angle in the sky, ignoring the overall shape and size of the source. Determining the change in shape between the source/image pair requires a more detailed mapping that calculates small changes in the position of numerous light rays in the image and source planes. This is a somewhat more difficult task that requires numerical methods, which is beyond the scope of the present work. However, treating the gravitational lensing terms as field variables is extremely useful and the benefits it purveys are three-fold:

(i) It allows us to determine differences in the global gravitational lensing properties from various realistic density distributions (in particular see figure 2 below).

(ii) We can determine the relevant lensing terms (convergence, shear, first- or second-flexion) for discerning between individual shapes of density profiles. For example in section 4 we show that convergence and first-flexion are good indicators of the Sérsic shape parameter, whereas the concentration of NFW profiles can be determined by looking at the shear and second-flexion.

(iii) The derivation of analytic solutions is a critical first step towards studying flexion through multiple lens planes with arbitrary mass distributions.

This paper is set out as follows; In section 2 we systematically develop the two-dimensional thin-lens gravitational lens equation for an arbitrary, circularly symmetric matter distribution, deriving the first-order terms in section 2.2 and the flexion terms in section 2.3. In section 3 we consider exact forms of the matter distributions, writing down analytic expressions for the convergence, shear and flexion for a point mass, singular isothermal sphere (SIS), NFW and Sérsic profiles in sections 3.1, 3.2, 3.3 and 3.4 respectively. In this way we are providing a single resource where the analytic forms for the convergence, shear, first- and second-flexion can be

ing, which they term *sextupole* lensing with components *sextupole*, *cardioid* and *displacement*. In Irwin et al. (2007) the authors show that sextupole is equivalent to second-flexion and a combination of the cardioid and displacement terms is equivalent to first-flexion.

<sup>2</sup> Galaxies are not intrinsically flexed providing they are dynamically relaxed.

found for a range of useful density profiles. Finally, in section 4 we compare the gravitational lensing effects of each of these profiles. We find that the shear and second-flexion for a Sérsic-law profile are systematically greater than for NFW and SIS profiles, whereas the convergence and first-flexion of each of the profiles are comparable. We further show that the convergence and first-flexion provide excellent tracers for the Sérsic shape parameter, whereas the shear and second-flexion are better indicators of the concentration parameter for the NFW profile. We make some concluding remarks in section 5.

## 2 ANALYTIC LENSING FORMALISM

### 2.1 The Thin-Lens Equation

Given that flexion considers finite source sizes, we require a two-dimensional version of the thin-lens gravitational lens equation, whereby the mapping between a point on the source plane and the image plane are explicitly expressed. In this way the thin-lens gravitational lens equation is expressed as

$$\eta_i = \frac{D_S}{D_L} \xi_i - D_{LS} \tilde{\alpha}_i, \quad (1)$$

where  $\xi_i$  is the impact parameter on the image plane,  $\eta_i$  is the distance between the origin of the coordinate system and the source on the source plane,  $\tilde{\alpha}_i$  is the deflection angle and  $D_S$ ,  $D_L$  and  $D_{LS}$  are the angular diameter distances from the observer to the source, the observer to the lens and the lens to the source respectively (the lens configuration is shown in figure 1). Equation (1) can be put into a neater form by using angular coordinates,  $\beta_i = \eta_i/D_S$  and  $\theta_i = \xi_i/D_L$ , such that

$$\beta_i = \theta_i - \alpha_i, \quad (2)$$

where  $\alpha_i = \tilde{\alpha}_i D_{LS}/D_S$  is the scaled deflection angle. Equation (2) can be re-expressed as a coordinate map between the two angular coordinate systems allowing the mapping to be expressed as a linear transformation

$$\beta_i = A_{ij} \theta_j, \quad (3)$$

where  $A_{ij} := \partial\beta_i/\partial\theta_j$  is the Jacobian of transformation and summation is assumed over repeated indices. Equation (3) implicitly assumes there are no gradients in the components of  $A_{ij}$  across the image. Physically, this implies that the convergence and shear are constant across the image, which is not necessarily a good approximation when the source has a finite spatial extent. This is a reasonable assumption if sources are assumed to be point-like, however for realistic cosmology one would like to be able to probe deviations of the shear and convergence across images. Goldberg & Bacon (2005) therefore generalized equation (3) to include higher-order terms, coined *flexion*. These flexion terms account for an image’s “arciness”, and are therefore relevant if one is considering sources of finite spatial extent. The non-linear expansion of the thin-lens equation is

$$\beta_i = A_{ij} \theta_j + \frac{1}{2} D_{ijk} \theta_j \theta_k, \quad (4)$$

where

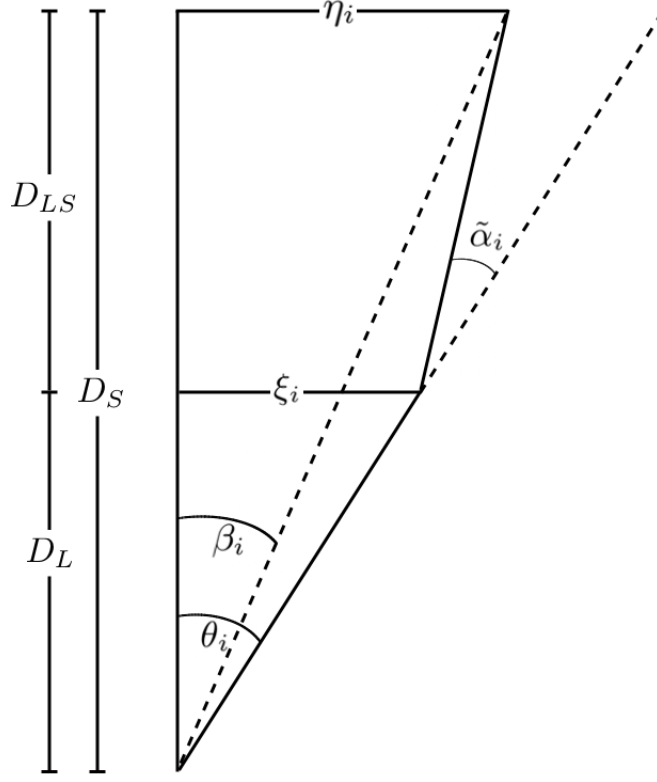


**Figure 1.** Lens configuration. Rather than use the angles,  $\theta_i$  and  $\beta_i$ , to describe the position of the image and the source on the lens plane respectively, we use the two-dimensional radial coordinates denoted  $\xi_i = D_L \theta_i$  and  $\eta_i = D_S \beta_i$ . The distances between the source plane, lens plane and observer are all measured in terms of angular diameter distances, and  $\tilde{\alpha}_i$  is the deflection angle.

$$D_{ijk} := \frac{\partial A_{ij}}{\partial \theta_k}, \quad (5)$$

is the gradient of the Jacobian. The components of the  $D_{ijk}$  matrix make up the components of the first- and second-flexion, a point that we discuss in considerably more detail in section 2.3.

We are interested in explicit expressions for the first- and second-order lensing terms with respect to positions on the image and source planes. It is therefore instructive for us to work in the Cartesian  $(\eta_i, \xi_i)$  system of coordinates rather than the angular  $(\beta_i, \theta_i)$  coordinates (see figure 1). In these coordinates, the Jacobian and its gradient are expressed as

$$A_{ij} = \frac{D_L}{D_S} \frac{\partial \eta_i}{\partial \xi_j} \quad \text{and} \quad D_{ijk} = \frac{D_L^2}{D_S} \frac{\partial^2 \eta_i}{\partial \xi_j \partial \xi_k}. \quad (6)$$

In this article, we restrict our attention to distributions of matter which are circularly symmetric when projected on to the lens plane. For such a profile, one can express the deflection angle as (see for e.g. Schneider 2006)

$$\tilde{\alpha}_i = \frac{4G}{c^2} \frac{M(|\xi|)}{|\xi|^2} \xi_i, \quad (7)$$

where  $|\xi| = \sqrt{\xi_1^2 + \xi_2^2}$  and the projected mass,  $M$ , is defined as the area integral of the surface density,  $\Sigma(|\xi|)$ , which for circular symmetry is given by

$$M(|\xi|) = 2\pi \int_0^{|\xi|} \Sigma(\xi') \xi' d\xi'. \quad (8)$$

Equation (1) can now be expressed in component form, also substituting equation (7), yielding

$$\eta_i = \xi_i \frac{D_S}{D_L} \left[ 1 - \frac{1}{\pi \Sigma_{cr}} \frac{M(|\xi|)}{|\xi|^2} \right], \quad (9)$$

where the critical surface density has been defined according to

$$\Sigma_{cr} = \frac{c^2}{4\pi G} \frac{D_S}{D_L D_{LS}}. \quad (10)$$

## 2.2 First-Order Lensing

The first-order Jacobian,  $A_{ij}$ , can now be calculated by differentiating equation (9) which, after some algebra is

$$A_{11} = 1 - \frac{2\Sigma(|\xi|)\xi_1^2}{\Sigma_{cr}|\xi|^2} + \frac{M(|\xi|)}{\pi\Sigma_{cr}|\xi|^4} (\xi_1^2 - \xi_2^2), \quad (11)$$

$$A_{22} = 1 - \frac{2\Sigma(|\xi|)\xi_2^2}{\Sigma_{cr}|\xi|^2} + \frac{M(|\xi|)}{\pi\Sigma_{cr}|\xi|^4} (\xi_2^2 - \xi_1^2), \quad (12)$$

$$A_{12} = \frac{-2\xi_1\xi_2}{\pi\Sigma_{cr}|\xi|^4} Q(|\xi|) = A_{21}, \quad (13)$$

where for convenience we have defined the function

$$Q(\zeta) := \pi\Sigma(\zeta)\zeta^2 - M(\zeta). \quad (14)$$

The convergence and two components of the shear are expressed in terms of the components of the Jacobian as follows

$$\gamma_1 = -(A_{11} - A_{22})/2, \quad (15)$$

$$\gamma_2 = -A_{12}, \quad (16)$$

$$\kappa = 1 - (A_{11} + A_{22})/2. \quad (17)$$

Evaluating the convergence by substituting equations (11) and (12) into (17) implies

$$\kappa = \frac{\Sigma(|\xi|)}{\Sigma_{cr}}, \quad (18)$$

which is the familiar version of this equation (see for e.g. Schneider 2006). Evaluating the two components of the shear using equations (11-13) implies

$$\gamma_1 = \frac{\mathcal{Q}(|\xi|)}{\pi \Sigma_{cr} |\xi|^4} (\xi_1^2 - \xi_2^2), \quad (19)$$

$$\gamma_2 = \frac{2\mathcal{Q}(|\xi|)}{\pi \Sigma_{cr} |\xi|^4} \xi_1 \xi_2. \quad (20)$$

To compare the equations for the shear with a more familiar form, we convert the above equations from Cartesian coordinates,  $(\xi_1, \xi_2)$ , into polar coordinates on the lens plane,  $(R, \phi)$ , defined by  $\xi_1 = R \cos \phi$  and  $\xi_2 = R \sin \phi$ . This implies that the convergence and total shear,  $\gamma = \gamma_1 + i\gamma_2$ , are

$$\kappa = \frac{\Sigma(R)}{\Sigma_{cr}}, \quad (21)$$

$$\gamma = \frac{\mathcal{Q}(R)}{\pi \Sigma_{cr} R^2} e^{2i\phi} = |\gamma| \exp(2i\phi). \quad (22)$$

This is consistent with showing that the shear is a spin-two quantity, whereas the convergence is spin-zero.

Equations (21) and (22) give the convergence and shear distributions as a function of the mass profile of the galaxy. Whilst the convergence is only dependent on the surface density, the shear is also a function of the mass. This immediately gives the expected result for a point mass lens that the convergence is everywhere zero (except at the origin), whereas the shear is non-zero and goes as  $M/R^2$  (see section 3.1).

### 2.3 Flexion

The real interest in this article lies in the flexion terms, which are given by the second-order Taylor series expansion, equation (4). The three-tensor,  $D_{ijk}$ , is expressed in terms of the gradient of the linear Jacobian of transformation in equation (6) that, given equations (11-13), allows us to calculate the individual components of the three-tensor in terms of the coordinates  $\xi_1$  and  $\xi_2$ . After much algebra, one finds

$$D_{111} = \frac{2D_L \xi_1 (\xi_1^2 - 3\xi_2^2)}{\pi \Sigma_{cr} |\xi|^6} \mathcal{Q} - \frac{2D_L \xi_1^3}{\Sigma_{cr} |\xi|^3} \frac{d\Sigma}{d|\xi|}, \quad (23)$$

$$D_{211} = \frac{2D_L \xi_2 (3\xi_1^2 - \xi_2^2)}{\pi \Sigma_{cr} |\xi|^6} \mathcal{Q} - \frac{2D_L \xi_1^2 \xi_2}{\Sigma_{cr} |\xi|^3} \frac{d\Sigma}{d|\xi|}, \quad (24)$$

$$D_{221} = \frac{-2D_L \xi_1 (\xi_1^2 - 3\xi_2^2)}{\pi \Sigma_{cr} |\xi|^6} \mathcal{Q} - \frac{2D_L \xi_1 \xi_2^2}{\Sigma_{cr} |\xi|^3} \frac{d\Sigma}{d|\xi|}, \quad (25)$$

$$D_{222} = \frac{-2D_L \xi_2 (3\xi_1^2 - \xi_2^2)}{\pi \Sigma_{cr} |\xi|^6} \mathcal{Q} - \frac{2D_L \xi_2^3}{\Sigma_{cr} |\xi|^3} \frac{d\Sigma}{d|\xi|}, \quad (26)$$

where for the remainder of the article  $\Sigma = \Sigma(|\xi|)$ ,  $\mathcal{Q} = \mathcal{Q}(|\xi|)$  and  $M = M(|\xi|)$  unless otherwise explicitly stated. As shown by Bacon et al. (2006), the three-tensor,  $D_{ijk}$ , can be expressed as the sum of two other tensors,  $D_{ijk} = \mathcal{F}_{ijk} + \mathcal{G}_{ijk}$ , which can be written component-wise as

$$\mathcal{F}_{ij1} = -\frac{1}{2} \begin{pmatrix} 3\mathcal{F}_1 & \mathcal{F}_2 \\ \mathcal{F}_2 & \mathcal{F}_1 \end{pmatrix}, \quad (27)$$

$$\mathcal{F}_{ij2} = -\frac{1}{2} \begin{pmatrix} \mathcal{F}_2 & \mathcal{F}_1 \\ \mathcal{F}_1 & 3\mathcal{F}_2 \end{pmatrix}, \quad (28)$$

$$\mathcal{G}_{ij1} = -\frac{1}{2} \begin{pmatrix} \mathcal{G}_1 & \mathcal{G}_2 \\ \mathcal{G}_2 & -\mathcal{G}_1 \end{pmatrix}, \quad (29)$$

$$\mathcal{G}_{ij2} = -\frac{1}{2} \begin{pmatrix} \mathcal{G}_2 & -\mathcal{G}_1 \\ -\mathcal{G}_1 & -\mathcal{G}_2 \end{pmatrix}. \quad (30)$$

In the above,  $\mathcal{F} = \mathcal{F}_1 + i\mathcal{F}_2$  and  $\mathcal{G} = \mathcal{G}_1 + i\mathcal{G}_2$  are known as first- and second-flexion respectively (Bacon et al. 2006). First-flexion is a spin-one quantity that measures the shift in the centroid of the image, and second-flexion is a spin-three quantity measuring the ‘‘arciness’’ of the image.

Inverting the above system of equations implies we can express the components of the first- and second-flexion in terms of the components of  $D_{ijk}$ ;

$$\mathcal{F}_1 = -\frac{1}{2}(D_{111} + D_{221}), \quad (31)$$

$$\mathcal{F}_2 = -\frac{1}{2}(D_{211} + D_{222}), \quad (32)$$

$$\mathcal{G}_1 = -\frac{1}{2}(D_{111} - 3D_{221}), \quad (33)$$

$$\mathcal{G}_2 = -\frac{1}{2}(3D_{211} - D_{222}). \quad (34)$$

Therefore, utilizing equations (23-26), (31) and (32), one can show that the components of the first-flexion are

$$\mathcal{F}_1 = \frac{D_L}{\Sigma_{cr}} \frac{\partial \Sigma}{\partial \xi_1}, \quad (35)$$

$$\mathcal{F}_2 = \frac{D_L}{\Sigma_{cr}} \frac{\partial \Sigma}{\partial \xi_2}. \quad (36)$$

That is, the first and second components of first-flexion (i.e.,  $\mathcal{F}_1$  and  $\mathcal{F}_2$  respectively) are the directional derivatives of the surface density. Note that the first-flexion terms do not include any functions of the mass, which is again consistent with the flexion due to a point mass being zero (see section 3.1). The total first-flexion,  $\mathcal{F} = \mathcal{F}_1 + i\mathcal{F}_2$ , is given by

$$\begin{aligned} \mathcal{F} &= \frac{D_L}{\Sigma_{cr} |\xi|} \frac{d\Sigma}{d|\xi|} (\xi_1 + i\xi_2) \\ &= \frac{D_L}{\Sigma_{cr}} \frac{d\Sigma(R)}{dR} e^{i\phi}, \end{aligned} \quad (37)$$

implying the first-flexion is a spin-one field (Bacon et al. 2006) which is the gradient of the surface density. Given that the convergence is proportional to the surface density, this is an equivalent way of saying that the first-flexion is the gradient of the convergence.

Following the same procedure outlined above, one can show that the components of the second-flexion are

$$\mathcal{G}_1 = \frac{D_L \xi_1 (\xi_1^2 - 3\xi_2^2)}{\pi \Sigma_{cr} |\xi|^6} \left[ \pi \frac{d\Sigma}{d|\xi|} |\xi|^3 - 4\mathcal{Q} \right], \quad (38)$$

$$\mathcal{G}_2 = \frac{D_L \xi_2 (3\xi_1^2 - \xi_2^2)}{\pi \Sigma_{cr} |\xi|^6} \left[ \pi \frac{d\Sigma}{d|\xi|} |\xi|^3 - 4\mathcal{Q} \right]. \quad (39)$$

These form the total second-flexion term,  $\mathcal{G} = \mathcal{G}_1 + i\mathcal{G}_2$ , as

$$\mathcal{G} = \frac{D_L}{\pi \Sigma_{cr} |\xi|^6} \left[ \pi \frac{d\Sigma}{d|\xi|} |\xi|^3 - 4\mathcal{Q} \right] (\xi_1 + i\xi_2)^3. \quad (40)$$

Finally, expressing the second-flexion in polar coordinates and expanding  $\mathcal{Q}$  to show the explicit dependence on the surface mass density and the projected mass one finds

$$\mathcal{G} = \frac{D_L}{\Sigma_{cr}} \left[ \frac{d\Sigma(R)}{dR} - \frac{4\Sigma(R)}{R} + \frac{4M(R)}{\pi R^3} \right] e^{3i\phi}. \quad (41)$$

This expression is relatively simple and shows the dependence of second-flexion on the surface density, its divergence and the projected mass distribution. Moreover, one can explicitly see that this is a spin-three field, as shown in Bacon et al. (2006).

It is pertinent to note that Schneider & Er (2008) showed that first- and second-flexion are not observable quantities due to the mass-sheet degeneracy. Instead, they showed that the observable spin-one and spin-three fields are the *reduced flexion* terms;

$$\frac{\mathcal{F} + g\mathcal{F}^*}{1 - \kappa} \quad \text{and} \quad \frac{\mathcal{G} + g\mathcal{F}}{1 - \kappa}, \quad (42)$$

where  $g = \gamma/(1 - \kappa)$  is the reduced shear and  $\mathcal{F}^* = \mathcal{F}_1 - i\mathcal{F}_2$  is the complex conjugate of first-flexion. Whilst it is beneficial to keep the mass-sheet degeneracy in mind, a majority of work on measuring flexion in real images using either the shapelets (Refregier 2003; Refregier & Bacon 2003; Goldberg & Bacon 2005) or HOLICs (Okura et al. 2007, 2008; Goldberg & Leonard 2007) approaches have been based on decomposing the higher-order components of the images into  $\mathcal{F}$  and  $\mathcal{G}$ . Therefore, for this article we continue to focus on the flexion quantities,  $\mathcal{F}$  and  $\mathcal{G}$ , rather than the terms expressed in (42).

## 2.4 A Note On Units

The system of coordinates we are using in this article are somewhat unconventional in the sense that they use distance, rather than angular coordinates on the image and source planes. We do this as we believe these units are more conducive to numerical applications, and are also more descriptive to the reader. However, our approach implies it is worth spending some time elucidating the dimensions that we are using for each of the derived quantities.

The surface density is defined as the projection of the three-dimensional density distribution, implying it has units of mass per unit area. Integrating this according to equation (8) implies the two-dimensional (projected) mass distribution has units of mass (as one would expect). Therefore, the convergence and shear given by equations (18), (19) and (20) are dimensionless. This is not surprising, and indeed this is true when one uses angular coordinates. The flexion terms presented here are in dimensions of (angle)<sup>-1</sup>, which is also consistent with those expressed in angular coordinates, however the angle is in units of radians. This can be seen as the expressions for the first- and second-flexion, equations (37) and (41) respectively, are proportional to the ratio of the angular diameter distance from the observer to the lens plane,  $D_L$ , and the impact parameter,  $|\xi|$ . As discussed in section 2.1, this ratio is  $\theta^{-1}$ . This implies that to compare the results presented in this paper with those derived using angular coordinates (for example Bacon et al. 2006), one must convert from units of radians to arcseconds. As an alternative, in appendix A we show the equations for convergence, shear and flexion expressed in angular coordinates.

## 3 EXACT SOLUTIONS

In this section we present analytic solutions of the equations expressed hitherto for various circularly symmetric matter distributions. For completeness, we first discuss the simplest case of a point mass, then move on to SIS, NFW and finally Sérsic-law profiles. These exact solutions are then used in section 4 to investigate differences between the flexion of various lenses, and we discuss how these flexion terms can be used to constrain the density distributions.

### 3.1 Point Mass

Consider a Schwarzschild lens (i.e. a point mass) situated at the origin of the coordinate system on the lens plane. This implies that  $\Sigma = \delta(|\xi|)$ , where  $\delta$  is the Dirac delta function. Moreover, the projected mass distribution  $M = M_s$  is a constant for all  $|\xi| \neq 0$ . The Einstein radius for such a system in angular coordinates is

$$\theta_E = \left( \frac{4GM_s}{c^2} \frac{D_{LS}}{D_S D_L} \right)^{1/2}, \quad (43)$$

and the critical surface density and Einstein radius are related according to

$$\Sigma_{cr} = \frac{M_s}{\pi D_L^2 \theta_E^2} = \frac{M_s}{\pi \xi_E^2}, \quad (44)$$

where we have defined  $\xi_E := D_L \theta_E$  to be the Einstein radius measured as a distance on the lens plane.

The convergence is linearly proportional to the surface density of the system, equation (18), implying it is trivially zero everywhere except  $|\xi| = 0$ . The shear, however, includes terms involving the projected mass of the system. From equations (19) and (20) the first and second components of the shear are

$$\gamma_1 = \frac{\xi_E^2}{|\xi|^4} (\xi_2^2 - \xi_1^2) \quad \text{and} \quad \gamma_2 = \frac{-2\xi_E^2}{|\xi|^4} \xi_1 \xi_2, \quad (45)$$

and the total shear is

$$\gamma = \frac{-\xi_E^2}{|\xi|^4} (\xi_1 + i\xi_2)^2 = \frac{-\theta_E^2}{\theta^2} e^{2i\phi}. \quad (46)$$

Note that the final equation in (46) is the usual expression for the shear associated with a point mass, however with an additional negative sign. This is a direct result of the calculation, however we note that the negative sign is due to the choice of coordinates. That is, rotating our coordinate system by ninety degrees implies the negative sign vanishes [i.e.  $\phi \rightarrow \phi + \pi/2$  implies  $\exp(2i\phi) \rightarrow -\exp(2i\phi)$ ]. Therefore, one is free to scale away the negative sign in equation (46) by rotating the coordinate system, which yields the familiar result for the shear induced by a point mass lens.

According to equations (35) and (36), the components of the first-flexion are the directional derivatives of the surface density, implying these vanish (for all  $|\xi| \neq 0$ );

$$\mathcal{F}_1 = \mathcal{F}_2 = \mathcal{F} = 0. \quad (47)$$

As mentioned above, first-flexion is associated with a shift of the centroid of the image with respect to the source. Therefore,  $\mathcal{F} \equiv 0$  for a point mass implies the centroid of the image is unchanged. Second-flexion, however, is associated with the ‘‘arciness’’ of the image, and one finds for the point

mass lens that

$$\mathcal{G}_1 = \frac{4D_L\xi_E^2}{|\xi|^6}\xi_1(\xi_1^2 - 3\xi_2^2), \quad (48)$$

$$\mathcal{G}_2 = \frac{4D_L\xi_E^2}{|\xi|^6}\xi_2(3\xi_1^2 - \xi_2^2). \quad (49)$$

Combining these, the total second-flexion is given by

$$\mathcal{G} = \frac{4D_L\xi_E^2}{|\xi|^6}(\xi_1 + i\xi_2)^3 = \frac{4\theta_E^2}{\theta^3}e^{3i\phi}. \quad (50)$$

Taking the magnitude of the above expression implies second-flexion decreases proportionally to the projected radius cubed,  $|\mathcal{G}| \propto |\xi|^{-3}$ , compared to the shear which decreases proportionally to the projected radius squared,  $|\gamma| \propto |\xi|^{-2}$ . Therefore, as one gets further from the source, the shear term will come to dominate over the second-flexion, and this effect will become more negligible as one looks further from the origin (see figure 2).

It is interesting to note that while the point mass has vanishing first-flexion and non-zero second-flexion, it is relatively straightforward to also construct lens models where the second-flexion vanishes but the first-flexion is non-zero. Indeed by setting equation (41) equal to zero, one can show that the second-flexion vanishes for models with  $\Sigma \propto |\xi|^2$ . Whilst this is obviously unphysical, as the surface density distribution increases monotonically as a function of radius, one still finds that the first-flexion is non-zero everywhere (for all  $|\xi| \neq 0$ ) with  $|\mathcal{F}| \propto |\xi|$ .

### 3.2 Singular Isothermal Sphere

Several observational studies of early-type galaxies using gravitational lensing have suggested that the total matter distribution (i.e. baryonic plus dark matter) is well described by a nearly isothermal density profile (Treu & Koopmans 2002, 2004; Rusin et al. 2003; Rusin & Kochanek 2005; Koopmans et al. 2006; Czoske et al. 2008; Dye et al. 2008; Tu et al. 2009). Indeed the strongest evidence for this is from Gavazzi et al. (2007) who reported weak lensing studies of 22 early-type galaxies based on *HST* imaging, concluding that an isothermal distribution is consistent out to 100 effective radii. On larger scales, isothermal spheres have been found to fit the density profile of galaxy clusters (Athreya et al. 2002; Ettori et al. 2002; Katgert et al. 2004), although recent debate has suggested the NFW profile may provide a better fit (see section 3.3). Analytically, gravitational lensing studies have compared SIS and NFW profiles at first- (Wright & Brainerd 2000) and higher-order (Bacon et al. 2006), implying the SIS profile provides us with the simplest realistic profile to reproduce known results.

The SIS density profile is described in terms of the three-dimensional (deprojected) radius,  $r$ , as

$$\rho(r) = \frac{\sigma^2}{2\pi G r^2}, \quad (51)$$

where  $\sigma$  is the one-dimensional velocity dispersion. Projecting equation (51) along the line-of-sight gives the surface density (for example see Binney & Tremaine 1987)

$$\Sigma = \frac{\sigma^2}{2G|\xi|}. \quad (52)$$

We note that the SIS profile, like the point mass, is singular at the origin. This implies that the following analysis is valid for all  $|\xi| \neq 0$ , however in reality one must quantify at what radius the system is a ‘‘weak lens’’ (see section 4). By defining the Einstein radius in units of distance as  $\xi_E := D_L\theta_E$ , where  $\theta_E$  is the standard Einstein radius for an SIS lens, one can show that the critical surface density,  $\Sigma_{cr}$ , is related to the Einstein radius as

$$\Sigma_{cr} = \frac{\sigma^2}{G\xi_E}. \quad (53)$$

By substituting the above equations into (18), we can show that the convergence falls-off linearly with the distance from the center of the coordinate system;

$$\kappa = \frac{\xi_E}{2|\xi|} = \frac{\theta_E}{2\theta}. \quad (54)$$

Moreover, the components of the shear have a similar behaviour with the extra angular dependence

$$\gamma_1 = \frac{-\xi_E}{2|\xi|^3}(\xi_1^2 - \xi_2^2), \quad (55)$$

$$\gamma_2 = \frac{-\xi_E}{|\xi|^3}\xi_1\xi_2. \quad (56)$$

As we know the shear is a spin-two field, we are essentially only interested in the strength of the respective fields. Therefore, for the remainder of the article, unless explicitly stated, we shall just be working with the magnitudes of these fields. Now, as  $\gamma = |\gamma|\exp(2i\phi)$ , one can show from the above that

$$|\gamma| = \frac{\xi_E}{2|\xi|} = \frac{\theta_E}{2\theta}. \quad (57)$$

The first-flexion components are

$$\mathcal{F}_1 = \frac{-D_L\xi_E}{2|\xi|^3}\xi_1 \quad \text{and} \quad \mathcal{F}_2 = \frac{-D_L\xi_E}{2|\xi|^3}\xi_2. \quad (58)$$

First-flexion is a spin-one field, implying  $\mathcal{F} = |\mathcal{F}|\exp(i\phi)$ . Equations (58) imply the first-flexion falls-off proportionally to the distance squared;

$$|\mathcal{F}| = \frac{-D_L\xi_E}{2|\xi|^2} = \frac{-\theta_E}{2\theta^2}. \quad (59)$$

The second-flexion components are

$$\mathcal{G}_1 = \frac{3D_L\xi_E}{2|\xi|^5}\xi_1(\xi_1^2 - 3\xi_2^2), \quad (60)$$

$$\mathcal{G}_2 = \frac{3D_L\xi_E}{2|\xi|^5}\xi_2(3\xi_1^2 - \xi_2^2), \quad (61)$$

which is a spin-three field,  $\mathcal{G} = |\mathcal{G}|\exp(3i\phi)$ , implying second-flexion also decreases proportionally to the radius squared

$$|\mathcal{G}| = \frac{3D_L\xi_E}{2|\xi|^2} = \frac{3\theta_E}{2\theta^2}. \quad (62)$$

All of the above equations that are written in angular coordinates are consistent with those presented in Bacon et al. (2006). These analytic expressions are plotted for a specific mass in figure 2 where they are compared with the NFW and Sérsic-law profiles.

### 3.3 Navarro-Frenk-White Profile

Compared to the SIS profile, the NFW profile introduces an extra parameter into the scaling of density distributions. The

concentration,  $c$ , which is defined as the ratio of the three-dimensional virial radius to the three-dimensional scale radius,  $c = r_\Delta/r_s$ , is a function of the particular cosmology being used. In section 4 we compare the NFW profile to the other profiles being analysed here, as well as comparing the effects of varying the concentration on the first- and higher-order lensing phenomena. The NFW profile is generally given in terms of the three-dimensional radii,  $r$ ,

$$\rho(r) = \frac{\delta_c \rho_c}{(r/r_s)(1+r/r_s)^2}, \quad (63)$$

where  $\rho_c$  is the critical density of the Universe and

$$\delta_c = \frac{\Delta}{3} \frac{c^3}{\ln(1+c) - c/(1+c)}. \quad (64)$$

Projecting this onto the two-dimensional radius,  $|\xi|$ , gives the surface density (Bartelmann 1996)

$$\Sigma = \frac{2\rho_c \delta_c r_s^3}{|\xi|^2 - r_s^2} [1 - \Xi(|\xi|)], \quad (65)$$

where we have defined the following function

$$\Xi(|\xi|) := \begin{cases} \frac{2r_s}{\sqrt{r_s^2 - |\xi|^2}} \operatorname{arctanh} \sqrt{\frac{r_s - |\xi|}{r_s + |\xi|}} & |\xi| < r_s \\ \frac{2r_s}{\sqrt{|\xi|^2 - r_s^2}} \operatorname{arctan} \sqrt{\frac{|\xi| - r_s}{|\xi| + r_s}} & |\xi| > r_s \end{cases}. \quad (66)$$

Integrating the surface density gives the projected mass distribution

$$M = 4\pi \rho_c \delta_c r_s^3 \left[ \ln \frac{|\xi|}{2r_s} + \Xi(|\xi|) \right]. \quad (67)$$

The convergence and shear can now be expressed simply as functions of the above expressions. From equation (21), the convergence is simply  $\kappa = \Sigma/\Sigma_{cr}$ , where the surface density is given by equation (65). The total shear is determined by equation (22) as

$$|\gamma| = \frac{2\rho_c \delta_c r_s^3}{\Sigma_{cr} (|\xi|^2 - r_s^2)} \left[ 1 - \Xi - 2 \left( 1 - \frac{r_s^2}{|\xi|^2} \right) \left( \ln \frac{|\xi|}{2r_s} + \Xi \right) \right], \quad (68)$$

where  $\Xi = \Xi(|\xi|)$ . Equation (37) implies first-flexion is found by differentiating the surface density, which can be shown to be

$$|\mathcal{F}| = \frac{-2D_L \rho_c \delta_c r_s^3}{\Sigma_{cr} |\xi| (|\xi|^2 - r_s^2)^2} (2|\xi|^2 + r_s^2 - 3|\xi|^2 \Xi), \quad (69)$$

and equation (41) implies the second-flexion for the NFW profile is given by the expression

$$|\mathcal{G}| = \frac{2D_L \rho_c \delta_c r_s^3}{\Sigma_{cr} |\xi| (|\xi|^2 - r_s^2)^2} \left[ 8 \left( 1 - \frac{r_s^2}{|\xi|^2} \right)^2 \ln \frac{|\xi|}{2r_s} + 3(r_s^2 - 2|\xi|^2) + \left( 15|\xi|^2 - 20r_s^2 + 8 \frac{r_s^4}{|\xi|^2} \right) \Xi \right] \quad (70)$$

Despite the mass of the system being infinite, one can show that the convergence, shear, first- and second-flexion all tend to zero as  $|\xi| \rightarrow \infty$ . These profiles are plotted against the SIS and Sérsic-law profiles in figure 2, and we also look at the dependence of the concentration in figure 3 and section 4.

### 3.4 Sérsic Profile

It has long been argued that a Sérsic-law (Sérsic 1968) provides a remarkably good fit to luminosity profiles of early-type galaxies, ranging in size from dwarf galaxies to the largest elliptical galaxies (Caon et al. 1993; Graham 2001; Graham & Guzmán 2003; Graham et al. 2003; Trujillo et al. 2004). For a concise reference to Sérsic quantities, see Graham & Driver (2005). Recently, a Sérsic-law has also been shown to provide a good fit to three-dimensional density profiles (Navarro et al. 2004), and also to projected surface density profiles (Merritt et al. 2005) of dark matter halos. In a series of papers (Merritt et al. 2006; Graham et al. 2006a,b) it has further been shown that projected Sérsic surface density profiles provide the best fit to simulated galaxy- and cluster-sized dark matter halos.

Cardone (2004) first analysed the Sérsic profile in the gravitational lensing context, showing that mass estimates using lens reconstructions is highly dependent on the choice of Sérsic parameter. Elíasdóttir & Möller (2007) compared gravitational lensing for Sérsic and NFW profiles, and found that mass estimates may differ by up to a factor of two, dependent on the choice of density profile and Sérsic index. In the weak lensing regime, they did this by looking at the shear of both profiles. We take this a step further by also analysing higher-order lensing terms. In this section, we provide the first explicit representation of flexion terms for the Sérsic-law profile, and in section 4 we compare these results to those of the NFW and SIS profiles.

The Sérsic profile is defined in terms of the surface density

$$\ln \left( \frac{\Sigma}{\Sigma_e} \right) = -b_n \left[ \left( \frac{|\xi|}{\xi_e} \right)^{1/n} - 1 \right], \quad (71)$$

where  $\Sigma_e$  is the surface density at the effective radius,  $\xi_e$ . The constant  $n$  is the Sérsic shape parameter which describes the shape of the profile and  $b_n$  is a function of  $n$  that is chosen such that the effective radius contains half of the projected mass of the system. Analytically, this is given as the solution of  $\Gamma(2n) = 2\Gamma(2n, b_n)$ , where

$$\Gamma(\alpha, x) = \int_{t=x}^{\infty} e^{-t} t^{\alpha-1} dt, \quad (72)$$

is the lower incomplete gamma function and  $\Gamma(\alpha) := \lim_{x \rightarrow \infty} \Gamma(\alpha, x)$  is the complete gamma function. As such,  $b_n$  can be reasonably approximated to  $b_n = 2n - 1/3 + 4/(405n) + \mathcal{O}(n^{-2})$  for  $0.5 < n < 10$  (Ciotti & Bertin 1999). Integrating the surface density gives the projected mass

$$M = 2\pi n \frac{e^{b_n}}{b_n^{2n}} \Sigma_e \xi_e^2 \Gamma(2n, Z), \quad (73)$$

where  $Z = b_n (|\xi|/\xi_e)^{1/n}$ . One can see that the Sérsic-law has one more parameter than the NFW profile, a point we discuss in more detail in section 4 and also appendix B.

After much algebra, one can show that the magnitudes of the convergence and shear for the Sérsic profile can be expressed as

$$\kappa = \frac{\Sigma_e}{\Sigma_{cr}} \exp \left\{ b_n \left[ 1 - \left( \frac{|\xi|}{\xi_e} \right)^{1/n} \right] \right\}, \quad (74)$$

$$|\gamma| = \frac{\Sigma_e}{\Sigma_{cr}} \left( \exp \left\{ b_n \left[ 1 - \left( \frac{|\xi|}{\xi_e} \right)^{1/n} \right] \right\} - \frac{2ne^{b_n} \xi_e^2}{b_n^{2n} |\xi|^2} \Gamma(2n, Z) \right). \quad (75)$$

Furthermore, the magnitudes of the first- and second-flexion terms are

$$|\mathcal{F}| = \frac{-D_L \Sigma_e b_n}{n \Sigma_{cr} |\xi|} \left( \frac{|\xi|}{\xi_e} \right)^{1/n} \exp \left\{ b_n \left[ 1 - \left( \frac{|\xi|}{\xi_e} \right)^{1/n} \right] \right\} \quad (76)$$

$$|\mathcal{G}| = \frac{D_L \Sigma_e}{\Sigma_{cr}} \left( \frac{8ne^{b_n} \xi_e^2}{b_n^{2n} |\xi|^3} \Gamma(2n, Z) - \frac{1}{|\xi|} \left[ \frac{b_n}{n} \left( \frac{|\xi|}{\xi_e} \right)^{1/n} - 4 \right] \times \exp \left\{ b_n \left[ 1 - \left( \frac{|\xi|}{\xi_e} \right)^{1/n} \right] \right\} \right). \quad (77)$$

#### 4 PROFILE COMPARISONS

We compare gravitational lensing effects of the various density distributions by holding the virial mass of each system constant, which is the same method used by Wright & Brainerd (2000) for comparing first-order lensing properties of the NFW and SIS profiles. The three-dimensional (i.e. deprojected) virial radius,  $r_\Delta$ , is defined as the radius inside which the average density of the halo is  $\Delta$  times the critical density of the Universe, implying the three-dimensional virial mass is  $M_\Delta = 4\pi\Delta\rho_{cr}^3/3$  (throughout the remainder of the article we use  $\Delta = 200$ ). Constructing the lens models then requires the three-dimensional (deprojected) density distribution for each profile, as well as the three-dimensional mass distribution. In general, these two equations can be inverted to find  $r_\Delta$ , and also the various parameters associated with the individual profiles (for example the velocity dispersion,  $\sigma$ , for the SIS profile). The Sérsic profile is a little more difficult to treat with this procedure as analytic forms of the deprojected density and mass functions do not exist. As such, we use the analytic approximations given by Prugniel & Simien (1997), as well as empirical relations from Graham et al. (2006b). Details of the way in which we construct Sérsic-law density distributions are provided in appendix B.

Following Bacon et al. (2006), we use a flat  $\Lambda$ CDM cosmology with  $\Omega_m = 0.3$ ,  $\Omega_\Lambda = 0.7$  and  $h = 0.72$ . We place the lensing mass at a redshift of  $z_L = 0.35$  and the source at  $z_S = 0.8$  as these values correspond to  $D_{LS}/D_S \simeq 0.5$ . To compare the four density profiles, we use a lens mass of  $M_{200} = 10^{12} h^{-1} M_\odot$ . For the NFW profile, the concentration factor,  $c$ , which is the ratio of the virial radius to the scale radius (see section 3.3), is a function of the cosmology and the redshift of the lens which, for the above system, is evaluated to be  $c = 7.20$ . For the Sérsic model we use empirically derived relations between the Sérsic shape parameter,  $n$ , and the mass of the system: from Graham et al. (2006b), their equation (12), we find the Sérsic shape parameter for a galaxy of mass  $M_{200} = 10^{12} h^{-1} M_\odot$  is  $n \simeq 8.6$ .

Figure 2 shows the lensing properties of the Schwarzschild lens (dotted red line), SIS (dashed green line), NFW (blue dashed-dot line) and Sérsic (thick black line)

mass distributions. The Schwarzschild lens has an Einstein radius of  $\xi_E \simeq 11.5$  kpc, which implies that for impact parameters inside this radius the results presented are not in the weak lensing regime. The most striking feature in these plots is that at large distances, the convergence and first-flexion for the SIS are significantly larger than for the NFW and Sérsic profiles. Bearing in mind that the convergence is linearly proportional to the surface density, this implies that at large distances the surface density of the SIS is also significantly larger than the NFW and Sérsic profile. This is consistent with the fact that the outer-logarithmic slope for NFW profiles is  $-3$ , while the slope of an isothermal sphere is  $-2$ . Additionally, the slope of a Sérsic-law profile depends on the specific shape parameter,  $n$ , and varies as a function of the distance from the centre of the profile, i.e.  $|\xi|$ . Interestingly, whilst these features are evident in the convergence and the first-flexion, they are less apparent in the shear and second-flexion.

It is worth exploring the extent to which the above properties of the NFW and Sérsic profiles depend on the concentration and shape parameters respectively. The concentration parameter in the NFW profile,  $c$ , is defined as the ratio of the virial radius to the scale radius, which is a function of the specific cosmology. Figure 3 shows the effect of a varying concentration on the different lensing properties. A lensing mass of  $M_{200} = 10^{10} h^{-1} M_\odot$  is used, with values of  $c = 4, 8, 12, 16, 20, 24$ . For a Schwarzschild lens of this mass at these distances the Einstein radius is  $\xi_E \simeq 1.2$  kpc, which again gives us a scale on which a weak lensing treatment is appropriate.

It is apparent from figure 3 that the lensing properties of an NFW profile are not linearly effected by the concentration parameter. Indeed as  $c$  becomes larger, the lensing properties begin to converge, implying that at large  $c$  the plots become indistinguishable. Moreover, the effect of the concentration parameter is greater at small distances from the centre of mass of the lensing galaxy. This is seen most pertinently in the convergence where at  $|\xi| \sim 10\xi_E$  the lines are indistinct. It is also interesting to note that variations in the concentration parameter cause the shear and second-flexion to change significantly more than the convergence and first-flexion. Therefore, given a series of lensed images, and assuming an NFW fit to the density profile, one can learn more about the specifics of the profile from the shear and the second-flexion than from the convergence and the first-flexion. There is likely to be a degeneracy between the mass of the lensing galaxy and the concentration parameter if there are only a handful of images. Our results imply that using both the shear and the second-flexion may be able to break this degeneracy so  $c$  and  $M$  can be obtained.

Figure 4 shows the lensing properties of Sérsic profiles for various values of the Sérsic shape parameter,  $n$ . The lensing mass is again  $M_{200} = 10^{10} h^{-1} M_\odot$ , implying the point mass lens has  $\xi_E \simeq 1.2$  kpc, and we vary  $1 \leq n \leq 9$ . The striking feature of these plots is that the shear and second-flexion have significantly less dependence on the shape,  $n$ , of the Sérsic profile than the convergence and the first-flexion. Indeed, zooming in on the vertical scale by an order of magnitude for the shear and second-flexion plots reveals that the dependence on  $n$  can only be seen for  $|\xi| \ll \xi_E$ . Moreover, the effect of the shape parameter on the convergence and first-flexion increases as one moves further from the source,



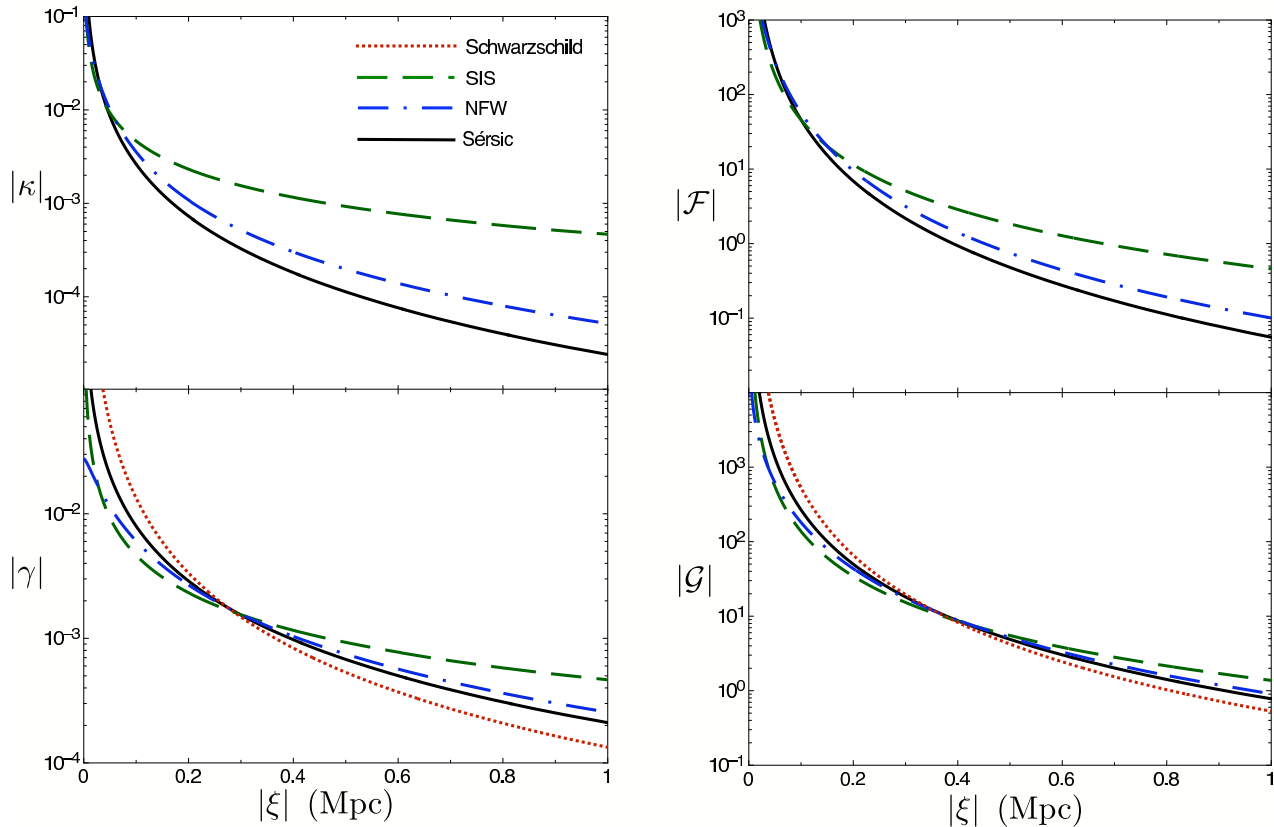


**Figure 2.** Convergence, shear, first- and second-flexion for Schwarzschild lens (dotted red line), SIS (dashed green line), NFW (dash-dot blue line) and Sérsic profile (thick black line). The three-dimensional virial masses of each of these profiles is  $10^{12}h^{-1}M_{\odot}$ , with the lens and source placed at  $z_L = 0.35$  and  $z_S = 0.8$  respectively. As an indicator of the weak lensing regime in these plots, the Einstein radius for the Schwarzschild lens is  $\xi_E \simeq 11.5$  kpc.

although this may be difficult to detect observationally due to the relative size of the signal being significantly weaker at large separations from the lensing mass. The fact that there is no dependence on the specific shape of the Sérsic profile on the shear and second-flexion implies that these two properties can be used to derive the mass of the lensing object, whilst the convergence and first-flexion can then be used to derive  $n$ . Weak gravitational lensing thus provides an independent method for deriving the masses of Sérsic-law galaxies and clusters which only weakly depends on the specific shape of the profile, provided the correct lensing properties are utilised, i.e. the convergence and second-flexion.

## 5 CONCLUSION

We have derived general equations governing the convergence, shear, first- and second-flexion for circularly symmetric gravitational lenses in terms of the surface density and projected mass of the lens. We have shown that the components of the first-flexion are simply the directional derivatives of the surface density, while the second-flexion is a slightly more complicated function of the surface density,

its gradient and also the projected mass distribution. By applying the formalism to specific lens models, in particular a Schwarzschild lens, a singular isothermal sphere (SIS), Navarro-Frenk-White (NFW) profile and a Sérsic profile, we have compared the signature each profile has on each of the lensing terms as a function of the radial impact parameter. Whilst the NFW and SIS profiles have been compared previously, both at linear-order (Wright & Brainerd 2000) and also for flexion (Bacon et al. 2006), to the best of our knowledge this is the first time flexion for Sérsic-law profiles have been presented. In particular, we showed that the shear and second-flexion effects for a Sérsic profile are systematically larger than for the NFW and SIS profiles (figure 2). This implies that one must be careful about the specific matter distribution assumed when attempting to analytically reconstruct the total mass and mass profile of a circularly symmetric lens.

An SIS profile is uniquely determined by designating the mass at a certain radius (e.g. virial mass). However, both the NFW and Sérsic models have extra parameters that determine their exact shape. The concentration of the NFW profile is the ratio of the virial radius to the scale radius, which is a function of the particular cosmology being

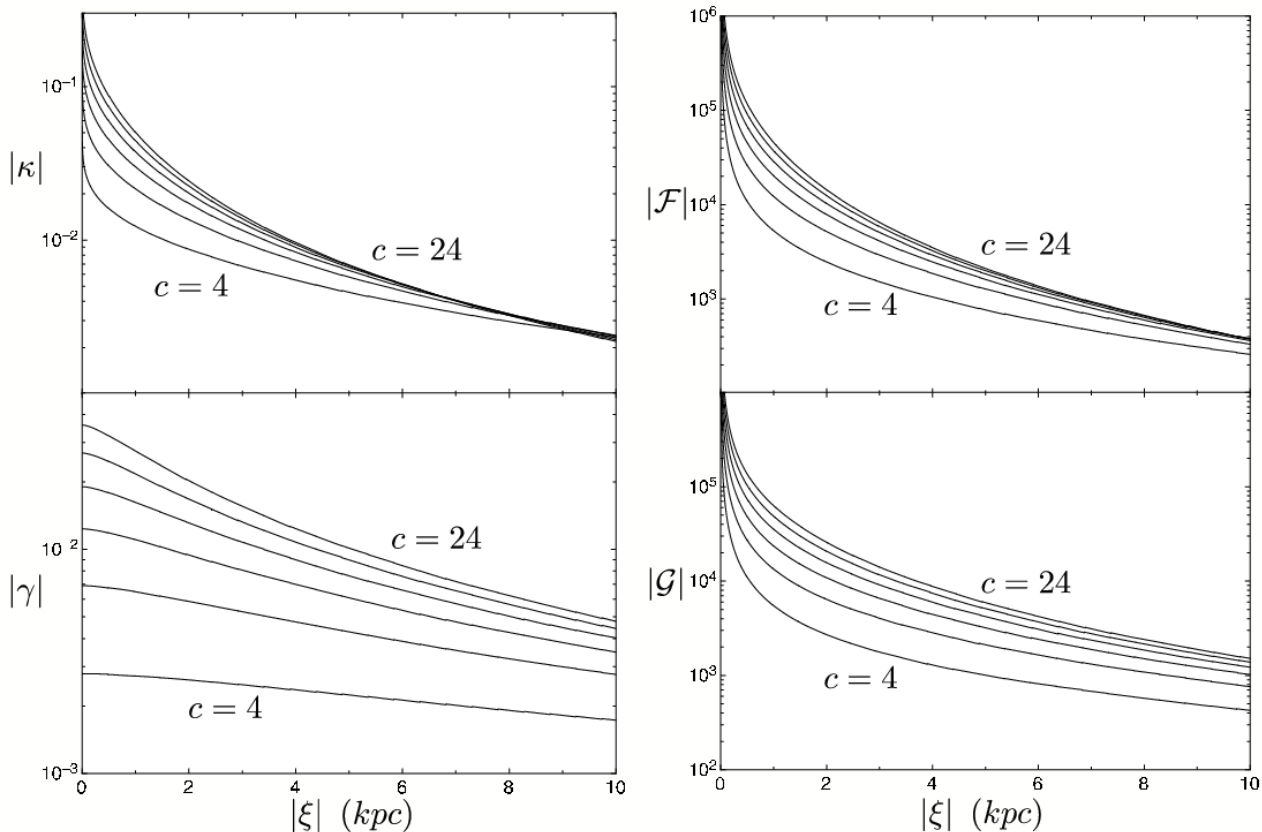


**Figure 3.** Convergence, shear, first- and second-flexion for NFW profiles with ranging values of the concentration,  $c$ , with  $M_{200} = 10^{10} h^{-1} M_{\odot}$ . Note that a Schwarzschild lens of this mass at this distance has an Einstein radius of  $\xi_E \simeq 1.2$  kpc, implying the weak lensing regime is somewhat beyond this limit. The values of the concentration shown are  $c = 4, 8, 12, 16, 20, 24$ . As the concentration increases, the curves converge on one another. The shear and the second-flexion show distinctions between the various values of the concentration better than the convergence and first-flexion.

considered. We showed that the convergence and first-flexion are relatively weakly dependent on the concentration parameter used, compared with the shear and the second-flexion (see figure 3). The Sérsic profile is parametrized by the Sérsic shape parameter,  $n$ . Counter to the NFW concentration parameter, the Sérsic shape parameter is more heavily dependent on the convergence and first-flexion, whereas the shear and second-flexion vary little as  $n$  changes (figure 4). These properties therefore provide the opportunity to directly measure both the mass of lensing galaxies as well as the specific shape of their density profiles. Given a limited supply of images around a specific galaxy, higher-order lensing terms may provide the ability to give extra constraints on the individual profiles of the galaxies.

The gravitational lensing systems explored in this article are idealized in that the projection of their mass distributions are circularly symmetric. Moving beyond circular symmetry requires the numerical solution of the thin-lens gravitational lens equation. One is then free to study the effect of non-circular lens models by including anisotropies in the lensing galaxy, and also to look at the effect the size of the source has on the shape of the final image. Whilst these

applications will be extremely useful for determining the mass distributions of various galaxies using next-generation gravitational lensing surveys, the higher-order gravitational lensing effects will also be useful in studying the dark matter and dark energy content of the Universe. Moreover, although the study of first-order gravitational lensing through N-body simulations has been around for some time (see for example the recent review by Munshi et al. 2008), the study of flexion in these systems has scarcely been broached. In this way, one can study the expected probability distributions for first- and second-flexion as a function of the specific cosmology. The advantage of using flexion as opposed to linear gravitational lensing effects is that a systematic bias is taken out of the study as only one reasonable assumption about the source object is required – that it is not intrinsically flexed.

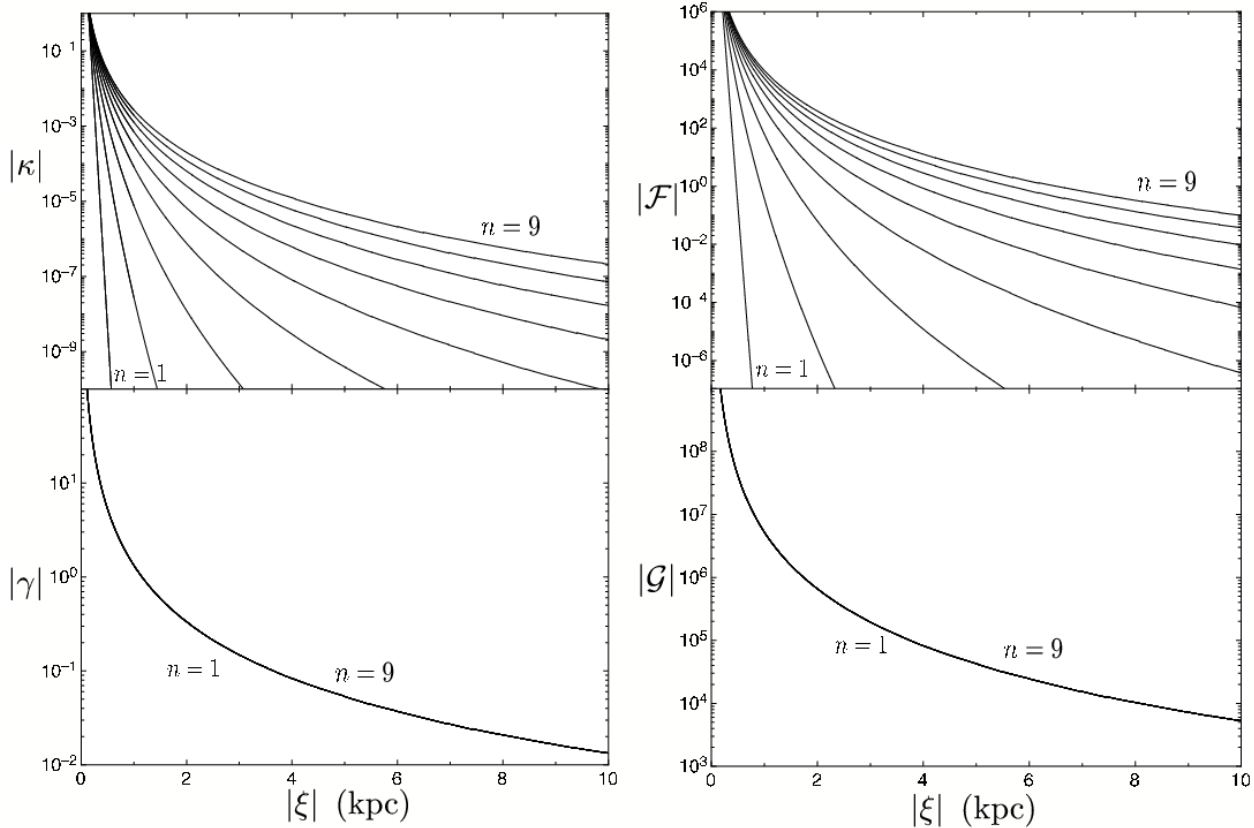


**Figure 4.** Convergence, shear, first- and second-flexion for Sérsic profiles with ranging values of the Sérsic shape parameter,  $n$ , with  $M_{200} = 10^{10} h^{-1} M_{\odot}$ . As with figure 3, a Schwarzschild lens of this mass at this distance would have an Einstein radius of  $\xi_e \simeq 1.2$  kpc, implying the weak lensing regime is somewhat beyond this limit. The shear and second-flexion vary extremely weakly with a change in  $n$ , whilst the convergence and first-flexion are more heavily dependent on this parameter.

## APPENDIX A: CONVERGENCE, SHEAR AND FLEXION IN ANGULAR COORDINATES

It is instructive to show the main equations from sections 2.2 and 2.3 expressed in angular coordinates,  $(\theta_1, \theta_2)$ , where  $\xi_i = D_L \theta_i$ . From the definition of the projected mass function in terms of the surface density, equation (8), implies that the projected mass expressed in angular coordinates is related to the mass in distance coordinates according to  $M(|\xi|) = D_L^2 M(|\theta|)$ , where  $|\theta| = \sqrt{\theta_1^2 + \theta_2^2}$ . It is trivial to show that the expression for the convergence, equation (18) goes unchanged, however the components of the shear, equations (19) and (20), written in angular coordinates become

$$\gamma_1(\theta_1, \theta_2) = \frac{\theta_1^2 - \theta_2^2}{\pi \Sigma_{cr} |\theta|^4} (\pi \Sigma |\theta|^2 - M) \quad (\text{A1})$$

$$\gamma_2(\theta_1, \theta_2) = \frac{2\theta_1\theta_2}{\pi \Sigma_{cr} |\theta|^4} (\pi \Sigma |\theta|^2 - M), \quad (\text{A2})$$

where for the remainder of this appendix  $\Sigma = \Sigma(|\theta|)$  and  $M = M(|\theta|)$ . The magnitude of the total shear is

$$|\gamma(\theta_1, \theta_2)| = \frac{1}{\pi \Sigma_{cr} |\theta|^2} (\pi \Sigma |\theta|^2 - M). \quad (\text{A3})$$

The components of the first-flexion, equations (35) and (36), are given in angular coordinates as

$$\mathcal{F}_1(\theta_1, \theta_2) = \frac{1}{\Sigma_{cr}} \frac{\partial \Sigma}{\partial \theta_1}, \quad (\text{A4})$$

$$\mathcal{F}_2(\theta_1, \theta_2) = \frac{1}{\Sigma_{cr}} \frac{\partial \Sigma}{\partial \theta_2}, \quad (\text{A5})$$

implying the magnitude of the first-flexion is

$$|\mathcal{F}(\theta_1, \theta_2)| = \frac{1}{\Sigma_{cr}} \frac{\partial \Sigma}{\partial |\theta|}. \quad (\text{A6})$$

Where previously the flexion terms were expressed in units of distance, one can now see first-flexion has units of  $(\text{angle})^{-1}$ . It is trivial to see that the following three expressions governing the second-flexion in terms of angular coordinates are also expressed in these same units.

$$\mathcal{G}_1(\theta_1, \theta_2) = \frac{\theta_1(\theta_1^2 - 3\theta_2^2)}{\pi \Sigma_{cr} |\theta|^6} \left[ \pi \frac{d\Sigma}{d|\theta|} |\theta|^3 - 4\pi \Sigma |\theta|^2 + 4M \right], \quad (\text{A7})$$

$$\mathcal{G}_2(\theta_1, \theta_2) = \frac{\theta_2(3\theta_1^2 - \theta_2^2)}{\pi \Sigma_{cr} |\theta|^6} \left[ \pi \frac{d\Sigma}{d|\theta|} |\theta|^3 - 4\pi \Sigma |\theta|^2 + 4M \right], \quad (\text{A8})$$

$$|\mathcal{G}(\theta_1, \theta_2)| = \frac{1}{\Sigma_{cr}} \left( \frac{d\Sigma}{d|\theta|} - \frac{4\Sigma}{|\theta|} + \frac{4M}{\pi |\theta|^3} \right). \quad (\text{A9})$$

## APPENDIX B: CREATING GALAXIES WITH SÉRSIC PROFILES

The Sérsic profile is defined in terms of the projected surface density, equation (71). However, to compare the lensing effects of the Sérsic profile with other density distributions, one requires the deprojected form of the density and mass distributions (see the discussion in section 4). Whilst an analytic form of the deprojected Sérsic profile is not available, an analytic approximation has been provided by Prugniel & Simien (1997), and has further been explored in detail by Merritt et al. (2006); Graham et al. (2006a,b).

Prugniel & Simien (1997) showed that the three-dimensional density distribution associated with the surface density of the Sérsic profile, given by equation (71), can be approximated as

$$\rho(r) = \rho_e \left(\frac{r}{\xi_e}\right)^{-p} \exp\left\{-b_n \left[\left(\frac{r}{\xi_e}\right)^{1/n} - 1\right]\right\}. \quad (\text{B1})$$

Here,  $\rho_e$  is the three-dimensional density at the effective (projected) radius  $\xi_e$ . The function  $p = p(n)$  is utilised to ensure that the projection of equation (B1) relates as closely as possible to the projected Sérsic profile, i.e. equation (71), for the range  $0.6 \leq n \leq 10$ . This was first given by Lima Neto et al. (1999) as  $p = 1.0 - 0.6097/n + 0.05463/n^2$ , and a goodness of fit is shown in Merritt et al. (2006). Integrating the three-dimensional density distribution over the volume gives the three-dimensional mass distribution,

$$M_{3D}(r) = 4\pi n \xi_e^3 \rho_e e^{b_n} b_n^{-(3-p)n} \Gamma\left[(3-p)n, b_n \left(\frac{r}{\xi_e}\right)^{1/n}\right]. \quad (\text{B2})$$

Cardone (2004) first looked at gravitational lensing for a Sérsic profile. He discussed the need to reduce the parameter space of the system in order to build a gravitational lens from a Sérsic model. To that end, he used an empirical relation governing the deprojected effective radius, the central surface brightness and the Sérsic shape parameter,  $n$  (see equation A.4 and A.5 of Cardone (2004)). It is possible for us to also use this relation, and subsequently convert the central surface brightness into a density by invoking more empirical relations and also assuming a mass-to-light ratio. Essentially, this procedure has already been completed for the Prugniel & Simien model by Graham et al. (2006b) [their equations (13) and (14)];

$$\log_{10} \rho_e = k - 2.5 \log_{10} \xi_e. \quad (\text{B3})$$

Here,  $\xi_e$  is in units of kiloparsecs,  $\rho_e$  is in solar masses per cubic parsec and  $k$  is a constant which is 0.5 for luminous elliptical galaxies and galaxy-sized dark matter halos (with  $\log R_e \gtrsim 0.5$ ) and 2.5 for cluster-sized dark matter halos (with  $\log R_e \gtrsim 1.5$ ). Finally, the three-dimensional density at the effective (projected) radius is related to the two-dimensional surface density at  $\xi_e$  by

$$\rho_e = \Sigma_e b_n^{(1-p)n} \frac{\Gamma(2n)}{2\xi_e \Gamma[(3-p)n]}. \quad (\text{B4})$$

As mentioned in section 4, to compare profiles we specify the virial mass of the system,  $M_\Delta$ , implying we know the virial radius,  $r_\Delta$ . Substituting this into equation (B2), together with equation (B3) implies we have an equation for  $\xi_e$  as a function of the Sérsic shape parameter,  $n$ . This equation is not analytically invertible due to the presence

of the incomplete gamma function, however it can be solved numerically for given values of  $n$ . Therefore, once this equation is solved, we know  $\xi_e$  and hence  $\rho_e$ , which can both be substituted into equation (B4) to give  $\Sigma_e$ . The projected Sérsic profile (71) can finally be evaluated, along with its various derivatives and also the two-dimensional mass, implying all of the lensing quantities can be evaluated.

## ACKNOWLEDGMENTS

We thank Alister Graham for helpful comments regarding the Sérsic profile and the Prugniel & Simien model. We also thank the referee for their extremely thorough and insightful review of the original manuscript. This research was supported under the Australian Research Councils Discovery Projects funding scheme (project number DP0665574).

## REFERENCES

- Athreya R. M., Mellier Y., Van Waerbeke L., Pelló R., Fort B., Dantel-Fort M., 2002, *Astron. Astrophys.*, 384, 743  
 Bacon D. J., Goldberg D. M., Rowe B. T. P., Taylor A. N., 2006, *Mon. Not. R. Astron. Soc.*, 365, 414  
 Bartelmann M., 1996, *Astron. Astrophys.*, 313, 697  
 Binney J., Tremaine S., 1987, *Galactic dynamics*. Princeton, NJ, Princeton University Press, 1987, 747 p.  
 Caon N., Capaccioli M., D’Onofrio M., 1993, *Mon. Not. R. Astron. Soc.*, 265, 1013  
 Cardone V. F., 2004, *Astron. Astrophys.*, 415, 839  
 Carlberg R. G., Yee H. K. C., Ellingson E., Morris S. L., Abraham R., Gravel P., Pritchet C. J., Smecker-Hane T., Hartwick F. D. A., Hesser J. E., Hutchings J. B., Oke J. B., 1997, *Astrophys. J.*, 485, L13  
 Ciotti L., Bertin G., 1999, *Astron. Astrophys.*, 352, 447  
 Côté P., Piatek S., Ferrarese L., Jordán A., Merritt D., Peng E. W., Hasegan M., Blakeslee J. P., Mei S., West M. J., Milosavljević M., Tonry J. L., 2006, *Astrophys. J. Supp.*, 165, 57  
 Czoske O., Barnabé M., Koopmans L. V. E., Treu T., Bolton A. S., 2008, *Mon. Not. R. Astron. Soc.*, 384, 987  
 Dye S., Evans N. W., Belokurov V., Warren S. J., Hewett P., 2008, *Mon. Not. R. Astron. Soc.*, 388, 384  
 Einasto J., 1965, *Trudy Inst. Astrofiz. Alma-Ata*, 5, 87  
 Elíasdóttir Á., Möller O., 2007, *J. Cosm. Astropart. Phys.*, 7, 6  
 Ettori S., De Grandi S., Molendi S., 2002, *Astron. Astrophys.*, 391, 841  
 Ferrarese L., Côté P., Jordán A., Peng E. W., Blakeslee J. P., Piatek S., Mei S., Merritt D., Milosavljević M., Tonry J. L., West M. J., 2006, *Astrophys. J. Supp.*, 164, 334  
 Gavazzi R., Treu T., Rhodes J. D., Koopmans L. V. E., Bolton A. S., Burles S., Massey R. J., Moustakas L. A., 2007, *Astrophys. J.*, 667, 176  
 Goldberg D. M., Bacon D. J., 2005, *Astrophys. J.*, 619, 741  
 Goldberg D. M., Leonard A., 2007, *Astrophys. J.*, 660, 1003  
 Goldberg D. M., Natarajan P., 2002, *Astrophys. J.*, 564, 65  
 Graham A. W., 2001, *Astron. J.*, 121, 820  
 Graham A. W., Driver S. P., 2005, *PASA*, 22, 118

- Graham A. W., Erwin P., Trujillo I., Asensio Ramos A., 2003, *Astron. J.*, 125, 2951
- Graham A. W., Guzmán R., 2003, *Astron. J.*, 125, 2936
- Graham A. W., Merritt D., Moore B., Diemand J., Terzić B., 2006a, *Astron. J.*, 132, 2701
- Graham A. W., Merritt D., Moore B., Diemand J., Terzić B., 2006b, *Astron. J.*, 132, 2711
- Hansen S. M., McKay T. A., Wechsler R. H., Annis J., Sheldon E. S., Kimball A., 2005, *Astrophys. J.*, 633, 122
- Hoekstra H., Jain B., 2008, *Annual Review of Nuclear and Particle Science*, 58, 99
- Hoekstra H., Yee H. K. C., Gladders M. D., 2004, *Astrophys. J.*, 606, 67
- Irwin J., Shmakova M., 2005, *New Astronomy Rev.*, 49, 83
- Irwin J., Shmakova M., 2006, *Astrophys. J.*, 645, 17
- Irwin J., Shmakova M., Anderson J., 2007, *Astrophys. J.*, 671, 1182
- Katgert P., Biviano A., Mazure A., 2004, *Astrophys. J.*, 600, 657
- Koopmans L. V. E., Treu T., Bolton A. S., Burles S., Moustakas L. A., 2006, *Astrophys. J.*, 649, 599
- Lauer T. R., Ajhar E. A., Byun Y., Dressler A., Faber S. M., Grillmair C., Kormendy J., Richstone D., Tremaine S., 1995, *Astron. J.*, 110, 2622
- Lauer T. R., Faber S. M., Gebhardt K., Richstone D., Tremaine S., Ajhar E. A., Aller M. C., Bender R., Dressler A., Filippenko A. V., Green R., Grillmair C. J., Ho L. C., Kormendy J., Magorrian J., Pinkney J., Siopis C., 2005, *Astron. J.*, 129, 2138
- Lima Neto G. B., Gerbal D., Márquez I., Capelato H. V., 1999, in Merritt D. R., Valluri M., Sellwood J. A., eds, *Galaxy Dynamics - A Rutgers Symposium Vol. 182 of Astronomical Society of the Pacific Conference Series*, Sérsic profile and specific entropy of elliptical galaxies. p. 211
- Lin Y., Mohr J. J., Stanford S. A., 2004, *Astrophys. J.*, 610, 745
- Lokas E. L., Wojtak R., Gottlöber S., Mamon G. A., Prada F., 2006, *Mon. Not. R. Astron. Soc.*, 367, 1463
- Mandelbaum R., Hirata C. M., Broderick T., Seljak U., Brinkmann J., 2006, *Mon. Not. R. Astron. Soc.*, 370, 1008
- Merritt D., Graham A. W., Moore B., Diemand J., Terzić B., 2006, *Astron. J.*, 132, 2685
- Merritt D., Navarro J. F., Ludlow A., Jenkins A., 2005, *Astrophys. J.*, 624, L85
- Munshi D., Valageas P., Van Waerbeke L., Heavens A., 2008, *Phys. Rep.*, 462, 67
- Navarro J. F., Frenk C. S., White S. D. M., 1997, *Astrophys. J.*, 490, 493
- Navarro J. F., Hayashi E., Power C., Jenkins A. R., Frenk C. S., White S. D. M., Springel V., Stadel J., Quinn T. R., 2004, *Mon. Not. R. Astron. Soc.*, 349, 1039
- Okabe N., Takada M., Umetsu K., Futamase T., Smith G. P., 2009, *LoCuSS: Subaru weak lensing study of 30 galaxy clusters*, arXiv:0903.1103
- Okura Y., Umetsu K., Futamase T., 2007, *Astrophys. J.*, 660, 995
- Okura Y., Umetsu K., Futamase T., 2008, *Astrophys. J.*, 680, 1
- Prugniel P., Simien F., 1997, *Astron. Astrophys.*, 321, 111
- Refregier A., 2003, *Mon. Not. R. Astron. Soc.*, 35, 338
- Refregier A., Bacon D. J., 2003, *Mon. Not. R. Astron. Soc.*, 338, 48
- Rines K., Diaferio A., 2006, *Astron. J.*, 132, 1275
- Rusin D., Kochanek C. S., 2005, *Astrophys. J.*, 623, 666
- Rusin D., Kochanek C. S., Keeton C. R., 2003, *Astrophys. J.*, 595, 29
- Schneider P., 2005, in Jetzer P., North P., eds, *Gravitational Lensing: Strong, Weak and Micro Weak gravitational lensing*. Springer-Verlag, Berlin
- Schneider P., 2006, in Meylan G., Jetzer P., North P., Schneider P., Kochanek C. S., Wambsganss J., eds, *Saas-Fee Advanced Course 33: Gravitational Lensing: Strong, Weak and Micro Part 1: Introduction to gravitational lensing and cosmology*. p. 1
- Schneider P., Er X., 2008, *Astron. Astrophys.*, 485, 363
- Sérsic J. L., 1968, *Atlas de Galaxias Australes*. Cordoba, Argentina: Observatorio Astronomico, 1968
- Treu T., Koopmans L. V. E., 2002, *Astrophys. J.*, 575, 87
- Treu T., Koopmans L. V. E., 2004, *Astrophys. J.*, 611, 739
- Trujillo I., Erwin P., Asensio Ramos A., Graham A. W., 2004, *Astron. J.*, 127, 1917
- Tu H., Gavazzi R., Limousin M., Cabanac R., Marshall P. J., Fort B., Treu T., Pello R., Jullo E., Kneib J. P., Sygnet J. F., 2009, *The mass profile of early-type galaxies in overdense environments: The case of the double source plane gravitational lens SL2SJ02176-0513*, arXiv:0902.4804
- van der Marel R. P., Magorrian J., Carlberg R. G., Yee H. K. C., Ellingson E., 2000, *Astron. J.*, 119, 2038
- Wojtak R., Lokas E. L., Mamon G. A., Gottlöber S., Prada F., Moles M., 2007, *Astron. Astrophys.*, 466, 437
- Wright C. O., Brainerd T. G., 2000, *Astrophys. J.*, 534, 34

This paper has been typeset from a  $\text{\TeX}$ / $\text{\LaTeX}$  file prepared by the author.